Soft Matter

Cell Motility, Contact Guidance, and Durotaxis

Journal:	*Soft Matter*
Manuscript ID	SM-ART-12-2018-002564.R1
Article Type:	Paper
Date Submitted by the Author:	03-May-2019
Complete List of Authors:	Feng, Jingchen; Rice University, center for theoretical biological physics Levine, Herbert; Rice University, Bioengineering; Rice University, Center for theoretical biological physics Mao, Xiaoming; University of Michigan, Physics Sander, Leonard; University of Michigan, Complex System; University of Michigan, Physics

Journal Name

ARTICLE TYPE

Cite this: DOI: 10.1039/xxxxxxxxxx

Cell Motility, Contact Guidance, and Durotaxis†

Jingchen Feng[a], Herbert Levine‡[a,b], Xiaoming Mao[c], and Leonard M. Sander‡[c,d]

Received Date
Accepted Date

DOI: 10.1039/xxxxxxxxxx

www.rsc.org/journalname

Mechanical properties of the substrate play a vital role in cell motility. In particular, cells have been shown to migrate along aligned fibers in the substrate (contact guidance) and up stiffness gradients (durotaxis). Here we present a simple mechanical model for cell migration coupled to substrate properties, by placing a simulated cell on a lattice mimicking biopolymer gels or hydrogels. In our model cells attach to the substrate via focal adhesions (FAs). As the cells contract, forces are generated at the FAs, determining their maturation and detachment. At the same time, the cell also allowed to move and rotate to maintain force and torque balance. Our model, in which the cells only have access to information regarding forces acting at the FAs, without a prior knowledge of the substrate stiffness or geometry, is able to reproduce both contact guidance and durotaxis.

1 Introduction

Motile eukaryotic cells can sense and react to the mechanical and structural properties of the substrate on which they move. An example of this is durotaxis: the tendency of cells to seek stiff tissue [1–5]. On fibrous substrates cells can sense another mechanical property, the alignment of the fibers, and they often follow the alignment. This is known as contact guidance [6,7].

It is generally thought that mechanical sensing occurs via the focal adhesions (FA) which attach the cell to the substrate. A direct bit of evidence for such sensing is the well-tested fact that FAs on stiff substrates are more likely to mature than on flexible ones [3,8]. Thus there are more FAs in stiffer regions. Cells almost certainly use this information to control their motility. In this paper we show that *both* contact guidance and durotaxis follow naturally from a model of cell motility that properly accounts for cell mechanics and incorporates the stiffness dependence of FA maturation to provide biological feedback. Our model applies to cell motion in two dimensions on various substrates but in principle could be extended to the case of 3d motion through a fibrous matrix.

We use two different models for the substrate on which the cells move. The simplest represents the hydrogels which are often used in experiment. For this case we construct a simple two-dimensional triangular lattice of links with bond-stretching and bond bending contributions to the energy. However, in real biological situations, cells move on fibrous biological gels such as collagen-I which are inhomogeneous and elastically nonlinear [9,10]. For this case we use a network model that shows features such as strain-induced alignment and strain-stiffening [11–14]. This network model uses a generalization of the triangular lattice constructed by removing a fraction of the bonds [15–17].

Our model for the mechanics of cell motion is based on a generalization of the work of Buenemann et al. [18] who considered forces and force balance in the motility cycle [19] of Dictyostelium discoideum. These authors assumed constant contraction rate during the contraction phase of the cycle and that the cell is connected to the substrate by adhesive bridges (intended to represent, for example, integrin) which are modeled as elastic springs. The bridges are located at the FAs. The formation of the attachments is homogeneous but detachment occurs at a spatially varying, force-dependent rate. Cell motion occurs at the point of the motility cycle when bridges in the back of the cell detach. Note that in this, as in all cell-motility problems, the motion is *quasi-static*: all forces on the cell balance, except for a brief interval after detachment, which causes the cell to change its center of mass and orientation so as to re-balance the force, as we discuss in detail below. Thus, in our model we assume that both the lattice and the cell are almost always in mechanical equilibrium. A strong prediction of this model is that the cell speed is largely independent of the value of the adhesive forces, which has been validated by experiment [20].

The model of Buenemann, et al. [18] is essentially one-dimensional: it does not consider the reorientation of the cell

[a]*Center for Theoretical Biological Physics, Rice University, 6100 Main Street, Houston, TX 77005-1892, USA*
[b]*Department of Bioengineering, Rice University, Houston, TX 77030-1402, USA*
[c]*Department of Physics, University of Michigan, Ann Arbor, Michigan 48109-1040, USA*
[d]*Center for the Study of Complex Systems, University of Michigan, Ann Arbor, Michigan 48109-1107, USA*
†Electronic Supplementary Information (ESI) available. See DOI: 10.1039/b000000x/
‡ Corresponding Authors: Herbert Levine: herbert.levine@rice.edu and Leonard M. Sander: lsander@umich.edu

during the migration process. However, in contact guidance and durotaxis cells are observed to turn in response to mechanical cues. To account for this we consider not only forces but also torques. In the course of the cell motion not only must forces (nearly) balance, but also torques. Also the substrate is taken to be homogeneous with a constant stiffness. In the present paper we generalize to the cases of alignment and spatial stiffness variation, and incorporate stiffness-dependent FA maturation.

Very little modeling effort has addressed contact guidance. Durotaxis, on the other hand has a substantial modeling literature. In one example of a durotaxis model[21,22] there is no mechanism for turning – torques are never considered. Furthermore, the elasticity of the substrate enters only as an effective "friction" which is intended to represent the breaking and reforming of bonds between the FAs and the substrate. Note that there is no way to account for alignment or non-linear elasticity in this formulation. Another treatment[23] evaluates the chemical and elastic free energy of a cell and linear substrate including recruitment of myosin motors. The assumed dynamics is not a motility cycle but rather over-damped motion down the gradient of the free energy. These authors assumed feedback of a different form from ours: it is in the stress dependence of the number of myosin motors which are active. This is a considerably more coarse-grained point of view than we take here. A treatment that shares more similarity with ours is Kim et al.[24]. These authors explore in detail how a filopod from a mesenchymal cell explores a fibrous mechanical environment and determines the changes in the polarization of the cell. The dynamics is encoded in the assumption that the cell follows the polarization. Thus this is a model for polarization rather than motility, and is complementary to what we present here.

2 Motility Model

In the model of Beunemann et al.[18], cells undergo a cycle of contraction and oriented protrusion. These processes create continuous transport of cell material to the front of the cell during the motility cycle. This idea is supported by the observation that cell speed is nearly a constant over the entire cycle and the motion of the cell outline appears to be that of continuous sliding[25].

In the model the cell body is assumed to contract uniformly with a constant rate during the contraction phase, whose duration is τ. Cell contraction is not hindered by viscous stress from the surrounding medium because external fluid drag is much, much smaller than the observed forces exerted on the substrate[26]. The adhesive bridges that connect the cell to the substrate form with a constant on-rate k_+ and break with a force- and position-dependent off-rate k_-. Their spring constants are denoted by k_s.

2.1 Two-dimensional Mechanical Model

In this work we take the assumptions above and generalize to two dimensions by also considering torque balance. The adhesion area of a cell is modeled as an ellipse with randomly distributed sites representing FAs. The position of the center of the ellipse is called $\boldsymbol{p}_m(t) = (x_m(t), y_m(t))$ and the positions of the FAs with respect to the center is $\boldsymbol{p}_i(t) = (x_i(t), y_i(t))$. The contraction is

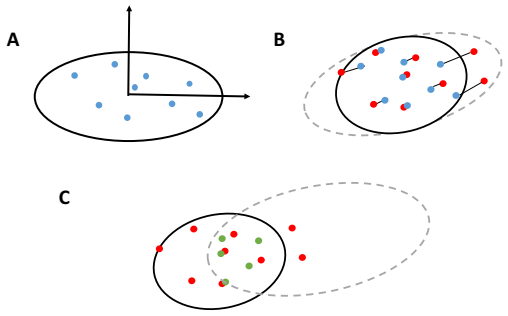

Fig. 1 Representation of cell-substrate adhesion during the contraction cycle. (a) The start of the contraction cycle. FAs are blue circles. The FAs form randomly at network nodes. (The network structure is not explicitly shown here.) (b) During the motility cycle, the cell contracts uniformly at a constant speed. The position of the attached network nodes is shown as red circles. The current position of FAs are blue circles. The contraction causes deformation of the network and rotation and shift of the cell. (c) The end of the contraction cycle: remaining FAs are shown in green. At the start of a new motility cycle, the cell outline is shifted such that its back coincides with last remaining adhesion site as indicated by the dashed ellipse.

represented by $\lambda = (A - A_\tau)/A$ where A, A_τ are the semimajor axes of the ellipse at the start and the end of the contraction. The contraction cycle is divided into 30 equal time steps dt (We have tried 50-time steps and the results are essentially the same). We assume the contraction only occurs along the long axis. The orientation of the cell at time t is called $\theta(t)$. Then, from simple geometry, the contraction dynamics of the node i is:

$$\begin{aligned} x_i(t+dt) &= x_i(t) - \lambda(dt/\tau)x_i(t)\cos^2\theta(t) \\ &\quad -\lambda(dt/\tau)y_i(t)\cos\theta(t)\sin\theta(t) \\ y_i(t+dt) &= y_i(t) - \lambda(dt/\tau)y_i(t)\sin^2\theta(t) \\ &\quad -\lambda(dt/\tau)x_i(t)\cos\theta(t)\sin\theta(t). \end{aligned} \tag{1}$$

At the beginning of the contraction phase, FAs are formed at each network node within the adhesion area with probability k_+. The force on a single FA is given by:

$$\boldsymbol{F}_i(t) = -k_s(\boldsymbol{R}_i(t) - \hat{\boldsymbol{R}}_i) \tag{2}$$

Here, $\boldsymbol{R}_i = \boldsymbol{p}_i + \boldsymbol{p}_m$ is the position of FA_i and $\hat{\boldsymbol{R}}_i$ the position of the network node. The total energy of the springs at the FAs at time $t+dt$ is:

$$E_s = \frac{k_s}{2}\sum_i [R_{d\theta}\boldsymbol{p}_i(t+dt) + \boldsymbol{p}_m(t+dt) - \hat{\boldsymbol{R}}_i)]^2 \tag{3}$$

Here $R_{d\theta}$ is the 2D rotation matrix through $d\theta$. The derivative of E_s with respect to θ is the net torque on the cell, and the derivative with respect to $\boldsymbol{p}_m(t+dt)$ is the net force on the cell. The cell center $\boldsymbol{p}_m$ and cell orientation θ are allowed to ensure zero net force and torque. At the same time, the network nodes $\hat{\boldsymbol{R}}_i$ are also allowed to move, minimizing the total energy of the cell and the network elasticity, as we discuss below.

Once the cell contracts, the traction forces on FAs will build up and a number of FAs will detach. In order to account for cell polarization, we need the attachments to be weaker (i.e. have a larger off-rate) at the back of the cell than in front. We encode this as follows:

$$k_-^{(0)}(x) = k_{-,b} - [k_{-,b} - k_{-,f}]\frac{x - x_b}{x_f - x_b}. \quad (4)$$

Here $x_{f/b}$ are the front/back of the cell at the start of the contraction cycle and $k_{-,f/b}$ are parameters with the constraint $k_b > k_f$.

The force dependence of the off-rate is modeled by Bell's law where the off-rate exponentially grows with the stretching [18,27]:

$$k_-(\boldsymbol{R}_i(t)) = k_-^{(0)}(x_i^0)\exp\left(\alpha\frac{|\boldsymbol{R}_i(t) - \hat{\boldsymbol{R}}_i|}{R}\right) \quad (5)$$

Here x_i^0 is the initial position of the FA along the major axes of the ellipse. The dimensionless parameter α measures the strength of the bond: see [18]. At the start of a new motility cycle, the cell outline is shifted such that its back coincides with last remaining adhesion site.

The bond attachment and detachment is treated with the kinetic Monte Carlo method. That is, after each time step bonds are broken and reformed with probability $k_\pm dt$.

This mechanical model is a very simplified version of real cell dynamics. The rigid rotation step, in particular, represents in an average way the rather complex process of protrusion of competing filopods. Our representation of a cell as an ellipse appears to be quite far from some cell types, e.g. fibroblasts, though it seems more plausible for more compact cell types such as glioma [28]. Presumably our approach will be best for such compact cells but will give us, we feel, qualitative insight for all cells. What this method cannot do is account in detail for the multiple, competing protrusions which are so prominent in fibroblasts. What we gain from this simplification is tractability of the model.

The network model that we use for biopolymer gels is known to reproduce many important features of fibrous matrices such as strain-induced alignment and strain-stiffening [11–14]. The network is built on a diluted triangular lattice as shown in Figure (2). Each bond in the lattice is present with a probability p. The probability p satisfies $pZ = \langle z \rangle$, where Z is the coordination number of the undiluted lattice ($Z = 6$ for triangular lattice), and z is the average connectivity of fibrous network. In experiment $\langle z \rangle \approx 3.4$ [29]. Therefore we study p in the range $[0.5, 0.65]$. We make contact with the mechanics of physical biopolymer gels by identifying the lattice sites as cross-linking points and bonds as fibrils between crosslinks. If bonds continue straight across a lattice site, they represent a continuing fiber. For simpler substrates such as hydrogels we simply put $p = 1$.

The elastic energy of the network is:

$$E_{net} = \sum_{<\alpha,\beta>}\frac{1}{2}k(\Delta l_{\alpha\beta})^2 + \sum_{<\alpha,\beta,\gamma>}\frac{1}{2}\kappa(\theta_{\alpha\beta\gamma})^2 \quad (6)$$

The sum $<\alpha,\beta>$ runs over bonds and $<\alpha,\beta,\gamma>$ runs over pairs of bonds that are co-linear and share lattice site j,and thus belong to the same fiber.

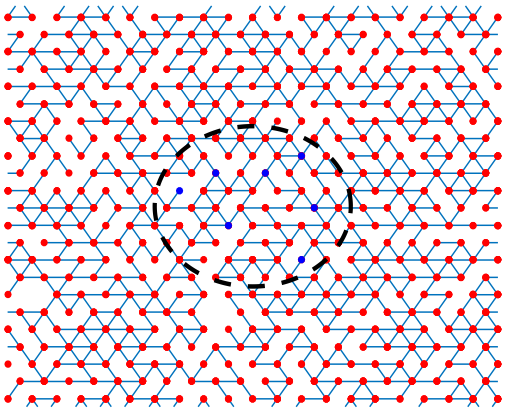

Fig. 2 The network model. The red circles are network nodes (crosslinking points) and the blue bonds are the fibrils between crosslinks. In the beginning of the contraction cycle, FAs (blue circles) have a probability to form on the top of each nodes within the adhesion area (dashed ellipse). Periodic boundary condition is applied to the network model in all the simulations

The length change of the bond is $\Delta l_{\alpha\beta}$, i.e.,

$$\Delta l_{\alpha\beta} = |\hat{\boldsymbol{R}}_\alpha(t) - \hat{\boldsymbol{R}}_\beta(t)| - l_0$$

where l_0 is the rest length of the bond. The angle $\theta_{\alpha\beta\gamma}$ is the angle between the adjacent bonds. The spring constant of the bonds is k and κ is the bending stiffness of the fibers. We always take $\kappa \ll kl_0^2$ for fibrous gels, in agreement with experiment. We use a 60x60 network in the results below. We have tested our results on networks of size up to 128 by 128 and obtained good consistency.

Cell contraction results in the displacement of the FAs, which leads to a nonzero net force and torque on the cell. To restore mechanical equilibrium we minimize the total energy of the system $E_{total} = E_s + E_{net}$ with respect to the position and orientation of the cell. That is, the cell (ellipse) is allowed to shift and rotate, and the network is allowed to deform.

2.2 Stiffness dependent maturation of focal adhesions

It is natural to extend the model of Buenemann et al. [18] by simply adding rotations. However, this will not do: it turns out that if this is all we do our simulated cells often migrate *down* the stiffness gradient. This is never observed and would be inconsistent with the idea that durotaxis has an important biological function [5] and hence needs to be robust in many biological environments. Clearly, we are missing a biological process.

We must incorporate the property of FAs mentioned above, namely that they are more likely to mature on stiff substrates [3,8]. For example, a recent experiment [8] shows that the local matrix microenvironment regulates the adhesion lifetime. It is positively correlated with the stiffness of the extra-cellular matrix. By inserting this effect into our model we make it robust for all the substrates we have examined.

In our study, the cell probes the local stiffness by contracting

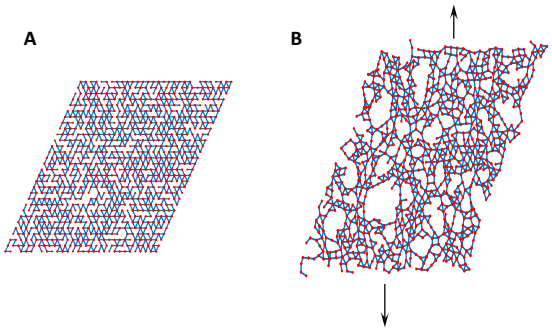

Fig. 3 Fiber alignment for contact guidance simulations. (a) The state of the network, which is isotropic before deformation. (b) Fibers are aligned along the stretching direction by external deformation. Here $p = 0.60$, $\kappa/k = 0.001$, stretching strain $\gamma = 0.40$.

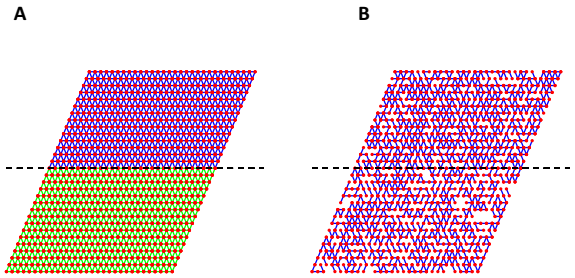

Fig. 4 Setting a stiffness gradient in the network model for a simulation of durotaxis. (a) Hydrogel case (p=1). $k_{upper} = 1.00$ (blue) and $k_{lower} = 0.001$ (green). (b) Fibrous network case. $p_{upper} = 0.65$ and $p_{lower} = 0.50$ The dashed line shows the location of the interface.

and the maturation of FAs depends on the traction forces between FAs and the substrate. Our model with FA maturation does show positive durotaxis as observed in experiments. It also shows that the orientation of the cell is along fiber alignments, which is consistent with experimental observations[6,7] of contact guidance.

In detail, instead of assuming all FAs survive after formation, we assume that nascent FAs are formed at each network node within the adhesion area with the probability k_+. At the end of the first time step dt, we determine if the FA will mature or perish based on the loading force on the FA. The maturation probability is taken to be:

$$p_m = 1 - k_m \exp\left(-\frac{|\boldsymbol{R}_i(t) - \hat{\boldsymbol{R}}_i^0|}{f_{threshold}}\right) dt. \quad (7)$$

Where $f_{threshold}$ is maturation force threshold. the For the rest of the contraction phase, mature FAs can detach from substrate at the end of each time increment, as we do in the basic model.

2.3 Fiber alignment and stiffness gradients

In order to study contact guidance we use the fact that gels have strain-induced alignment[11]. In the simulations we introduce fiber alignment by simply stretching the network: Figure (3).

For durotaxis we first simulate the case where cells are placed on top of a simple substrate such as hydrogel as in many *in vitro* experiments. We represent the hydrogel as a network with $p = 1$ and introduce a stiffness gradient by varying the spring constant k in space. To create a sharp jump in stiffness gradient, we take the upper half of the network to have k_{upper} and the lower half of the network k_{lower}: Figure (4a).

In contrast, for a biopolymer gel such as collagen, cells are placed on the top of the diluted network. We introduce a stiffness gradient by keeping k constant but spatially varying p – in effect we are modeling density variations in the gel. We create the sharp jump in by putting $p = p_{upper}$ in the upper p_{lower} in the lower part: Figure (4b).

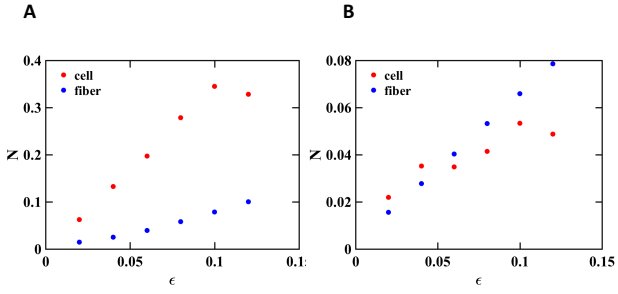

Fig. 5 Nematic order parameter N for cells and fibers. $p = 0.60$ and (a) $\kappa/k = 0.001$ (b) $\kappa/k = 1$. N_{cell} is calculated over 500 cell samples, and N_{fiber} is calculated over all fibers in each sample.

3 Results

3.1 Contact guidance

We first consider contact guidance, namely the tendency of cells to follow fiber orientation[6,7]. We stretch the network in the vertical direction with strain ε to induce fiber alignment. Then a cell is put on the substrate with a uniformly distributed orientation $\theta(t = 0)$. The simulation lasts for 50 cell cycles and the orientation of the cell is recorded at the end of the simulation. The simulation is repeated 500 times. To quantify the alignment, we calculate the nematic order parameter N for both cells and fibers in each samples. $N_{cell/fiber} = \langle \cos(2\theta) \rangle$, where θ is the direction of the cell/fiber orientation measured from the stretching direction. Figure 5a shows that both fiber alignment N_{fiber} and cell orientation N_{cell} are positively correlated with the stretching strain ε, confirming both strain-induced alignment and contact guidance.

Note that external strain induces both fiber alignment and stiffness anisotropy. To figure out which is important in contact guidance in our model, we test a slightly different case where the bending stiffness $\kappa = 1$ (Figure 5b). Interestingly, the strain-induced fiber alignment stays largely the same in this case, while N_{cell} is strongly suppressed. This observation suggests that the network geometry alone is not enough for contact guidance, because in both $\kappa = 1$ and $\kappa = 0.001$ cases we observe comparable

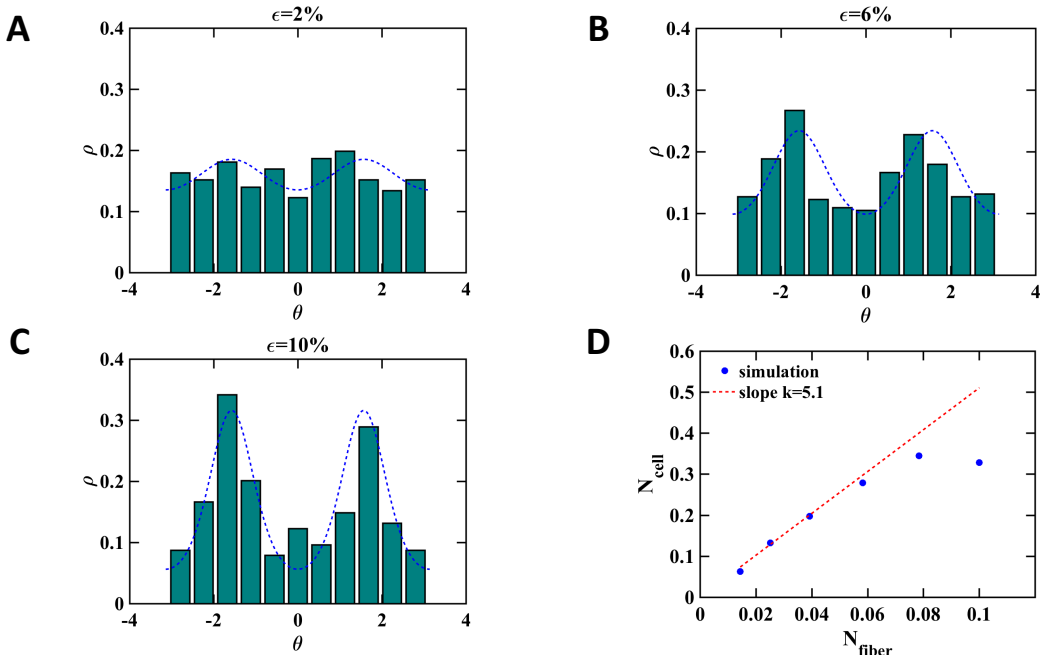

Fig. 6 (a)-(c) cell orientation distribution after 50 cell cycles. The blue line represents the results of Fokker-Planck equation with $k_c' = 11$ (See Supplementary Materials). Stretching strain (a) $\varepsilon = 2\%$ (b) $\varepsilon = 6\%$ (c) $\varepsilon = 10\%$. (d) nematic order of cell orientation versus nematic order of fiber alignment. The dashed line is a linear function with a slope of 5.1.

fiber alignment strength, but the cell orientation is quite different. A plausible explanation here is that the cell senses the stiffness of its environment by deforming it. When the network is too stiff to deform, the cell loses its ability to sense stiffness anisotropy, resulting in the weakening of the contact guidance. In cases where the geometry is very anisotropic, it is possible that contact guidance could occur from geometry alone[30]. Further, a more realistic treatment of filopods as in[24] might lead to additional geometry dependence; see the Discussion below.

The distribution of the cell orientation (Figure 6(a)-(c)) shows two peaks in the probability density function, illustrating cells' preference for moving along the fiber alignment direction. The x-axis is set to be $\theta = 0$. The two peaks occur at $\theta = \pm\pi/2$ i.e along the y- axis. The network is stretched along y-axis. Thus most cells are moving along the direction along which the network is stretched.

Such a distribution can also be understood with a Fokker-Planck equation (See Supplementary Materials). The dashed lines in Figure 6(a)-(c) are fitting results from the Fokker-Planck approach. This alternative Fokker-Planck treatment also gives consistent value of the initial slope of the curve N_{cell} vs. N_{fiber} to the simulations. We leave the discussion of Fokker-Planck approach to the Supplementary Material, because this approach does not explicitly consider the mechanical aspects of cell migration, which is the focus of this paper.

3.2 Durotaxis

We now turn to simulations which demonstrate durotaxis. We first test the hydrogel case ($p = 1$) where a sharp jump in stiffness is created by varying the spring constant k as in Figure (4). We start the cell on the interface with orientation parallel to the interface (positive x-axis direction). The simulation lasts for 15 cell cycles. At the end of the simulation, we record the location and the orientation of the cell.

We find that in the basic model (without FA maturation) the cell will move (albeit slightly) towards decreasing stiffness, which is the opposite of durotaxis (see Figure 7(a)). This is easy to understand: suppose a cell has four FAs at top left, top right, bottom left and bottom right respectively. The FAs feel traction forces from the network due to cell contraction, and the cell is in torque balance. At a certain point, the top left FA will break first, since the cell has a larger detachment rate at the rear and the stiff region causes a stronger stretching of the FAs. This breaking event will further causes torque imbalance. The cell needs to rotate clockwise to reach new torque balance (Figure 7(b)). FA maturation resolves this problem since more FAs mature in the stiff region. and the cell with can correctly sense and move towards the stiffer region (Figure 7(c)). In the following, we will use the full model with FA maturation unless otherwise stated (FA maturation does not affect contact guidance. The contact guidance results shown above is from the full model. But we observe similar results from the basic model).

Next we test the biopolymer network case. Figure (8) is an example of a cell (with FA maturation) moving on a substrate with a spatially varying stiffness obtained by varying p. Initially, the cell center is on the interface (Figure 8a). After two cell cycles, the cell moves rightwards but does not steer to the stiff region yet (Figure 8b). After four cell cycles, the cell reorients towards the stiff region (Figure 8c).

In Figure 9 we repeat the simulation 500 times and measure

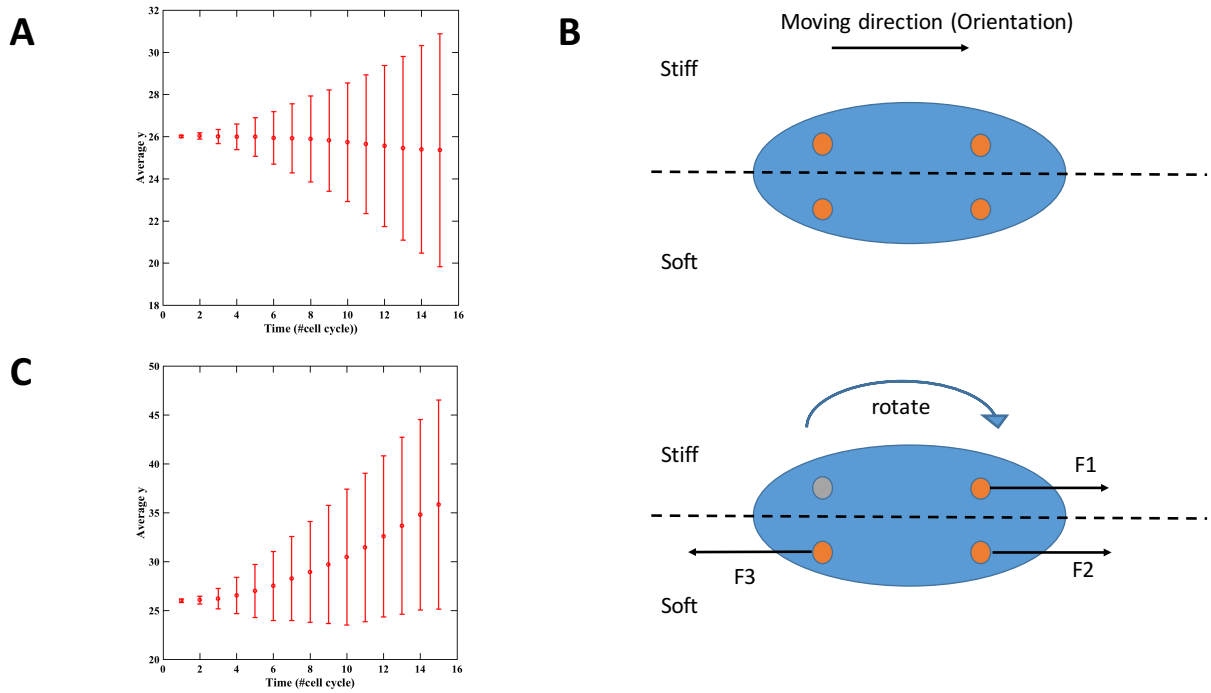

Fig. 7 Stiffness gradient by varying k. The average y coordinate as a function of time (a) The cell model without FA maturation shows negative durotaxis. (c) With FA maturation the cell moves towards the stiff (top) region. (b) Cell orientation change in the model without FA maturation.

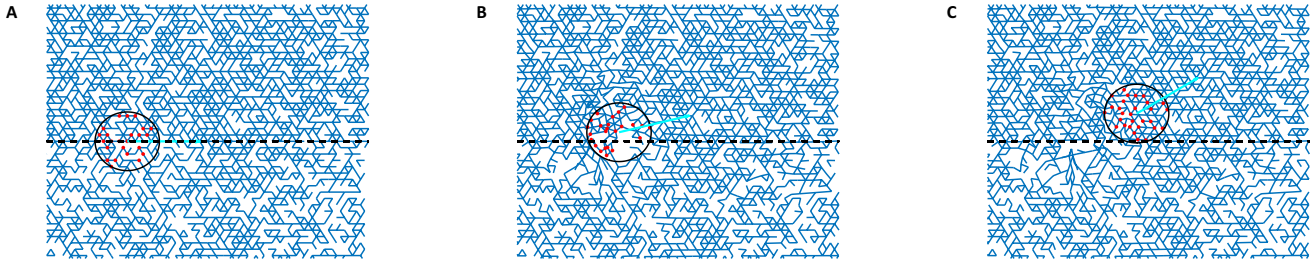

Fig. 8 An example of a cell (with FA maturation) migrating on a substrate with a spatially varying stiffness. (a) initial state; (b): third; (c); fifth cell cycle. The red dots represent focal adhesions. Dashed line shows the interface between the stiff substrate (top) and soft substrate (bottom). $p_{upper} = 0.65$, $p_{lower} = 0.50$, $\kappa/k = 0.001$. Arrows indicate the orientation of the cell. Note that in this example the cell is circular (radius equals 4 lattice spacing). The actual shape of the network is the same as in Figure 4. The right side of the network is pieced together with left side in the figures above, since the periodic boundary condition is applied.

the average coordinate of the cell, $\langle y \rangle$, and the distribution of cell orientations at the end of the simulation. It is clear that $\langle y \rangle$ and $\langle \theta \rangle$ is positively correlated with the stiffness gradient. The cell's ability is highly sensitive to stiffness gradients. For example, for $p_{upper} = 0.60$ and $p_{lower} = 0.55$, the geometry of the two sides of the network looks essentially the same (see Supplementary Materials). Nevertheless, the cell shows a strong preference to move up (Figure 9e). Since we use a large number of FAs the model integrates the stiffness information over the whole cell adhesion area and averages out the randomness. As a result, the cell shows a consistent tendency to move towards the stiff region.

One problem of varying bond occupation probability p to create a stiffness gradient is that the shear modulus dependence on p refers to a macroscopic phenomenon: at small length scales, a small difference in G is often overwhelmed by disorder. In order to treat small G differences as observed in experiment (such as two-fold over the size of the cell[18]), we test the case where the stiffness gradient is created by varying spring constant k of bonds (Figure 10 (a)). To mimic the stiffness gradient in experiments, the spring constant of the softer region is set to be 50% of the stiffer region. We set the initial orientation of cells to be the positive y direction. When cells move on the homogeneous substrates, the average velocity of cells in the y direction is roughly a constant, as the slope of the average y coordinate vs time is a constant (black curve in Figure 10 (b)). When cells start on stiffer region and move towards the softer region, the average velocity of cells in the y direction quickly slows down as cells approaches the interface, and most cells make sharp turns to avoid entering the softer region (red curve in Figure 10 (b)). Interestingly, if cells start on the softer region and move towards the stiffer region, the majority of cells fail to move out of the softer region and get trapped locally (blue curve in Figure 10 (b)). The results here confirm that our model is capable of showing durotaxis with a stiffness change similar to experiments.

It is worth noting that some experiments shows that cells can respond to not only sharp changes in stiffness, but also smooth changes[5,31]. To test if our model can predict similar phenomenon, we set a linear gradient of spring constant instead of a sharp interface, and keep all other setting the same as in Figure 10 (a). From the trajectory of cells (Figure 11(a)), we can clearly see that a large proportion of cells sense the existence of linear stiffness gradient and make turns to avoid moving into softer regions. This observation is further confirmed by the average y coordinate of cells vs time curve (Figure 11(b)). After five cell cycles, the average velocity of cells in the y direction approaches zero, which is in stark contrast to the uniform stiffness case (black curve in Figure 10 (b)).

Another interesting prediction of our model, for the case of biopolymer gels, is that cells are insensitive to the change of bending stiffness κ of the network (We tested κ/k ranging from 0.001 to 0.03. results not shown here). A possible explanation is that the strong cell contractions drive the local network into nonlinear region, which is dominated by stretching energy[13,14] and hence insensitive to κ. This result suggests that cells may not show durotaxis under a stiffness gradient created by spatially varying crosslink density for biopolymer gels.

4 Discussion

In this paper we present a simple mechanical model basing on the work of Buenemann et al. [18]. We generalize the model to two-dimensions by considering torque balance of the cell in addition to force balance. This naturally allows the cell in our model to re-orient during the migration. Consistent with experimental observations, our model exhibits re-orientation that is influenced by both fiber alignment and stiffness gradient. Our model also shows that FA formation, maturation and detachment play a critical role in determining the reorientation of the cell.

For contact guidance, an interesting question is whether geometrical anisotropy or mechanical anisotropy governs the effect. First, we need to emphasize that mechanical anisotropy is almost always inseparable from geometrical anisotropy. To give a simple example, consider a gel with all the fibers aligned in the horizontal direction. Clearly, in this situation, the gel is easier to deform in the vertical direction than the horizontal direction: that is, mechanical anisotropy originates from geometrical anisotropy. In our simulations, we varied the bending stiffness κ of the network to generate networks with similar geometry but different mechanical properties (Figure 8b). We observe that, in our model, contact guidance disappears in the large κ limit. Thus mechanical response and mechanical anisotropy is the fundamental cause of contact guidance in our picture. For actual (not idealized elliptical) cells, the situation might be different[24,30], probably because of competition between protrusions which is beyond the scope of our model. We can regard our work as a proof of principle that contact guidance *could* arise from anisotropy of stiffness.

Most experiments which reported durotaxis were conducted on hydrogels instead of biopolymer gels[1,31]. However, biopolymers constitute a major part of tissues. and it is important to consider their fibrous structure[32]. One difference between hydrogels and biopolymer gels is that biopolymer gels often have strong mechanical anisotropy[33].

To address both cases, we treat both hydrogels and biopolymer gels using lattice-based models with different bond occupation probability. We find that FA maturation is indispensable for the case of durotaxis on hydrogels. In fact, we show with our simple model that the cell would prefer to move along the descending direction of stiffness in the absence of FA maturation. With FA maturation, our model shows durotaxis under stiffness gradient created by different mechanisms, including spatially varying bond occupation probability p and spatially varying spring constant k. In addition, cells in our model can respond to not only sharp interface, but also smooth stiffness changes. Importantly, the change of stiffness in our model is comparable to that in experiment. All these observations confirm the usefulness of our model in explaining the formation of durotaxis.

So far, we have only considered single-cell properties, as this is already computationally challenging. Of course, inclusion of substrate mechanics immediately .gives rise to long-range cell-cell interactions; these then need to included along with direct interactions via adhesion proteins.. Future work will consider multicellular systems and the roles of guidance and/or durotaxis for collective motion.

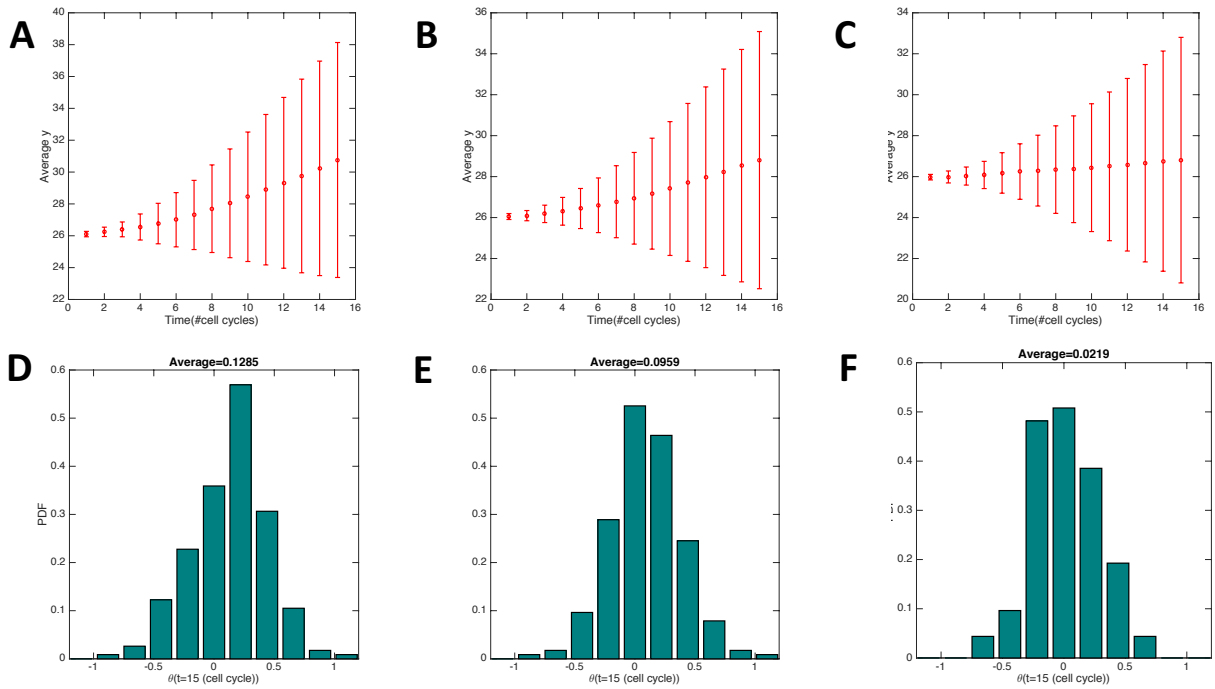

Fig. 9 Stiffness gradients guide cell migration. (a)-(c) Average y coordinate of the cells versus time. (d)-(f) Distribution of cell orientations. Parameters: $\kappa/k = 0.001$, (a) and (d) $p_{upper} = 0.65$, $p_{lower} = 0.50$. (b) and (e) $p_{upper} = 0.60$, $p_{lower} = 0.55$. (c) and (f) $p_{upper} = 0.58$, $p_{lower} = 0.57$

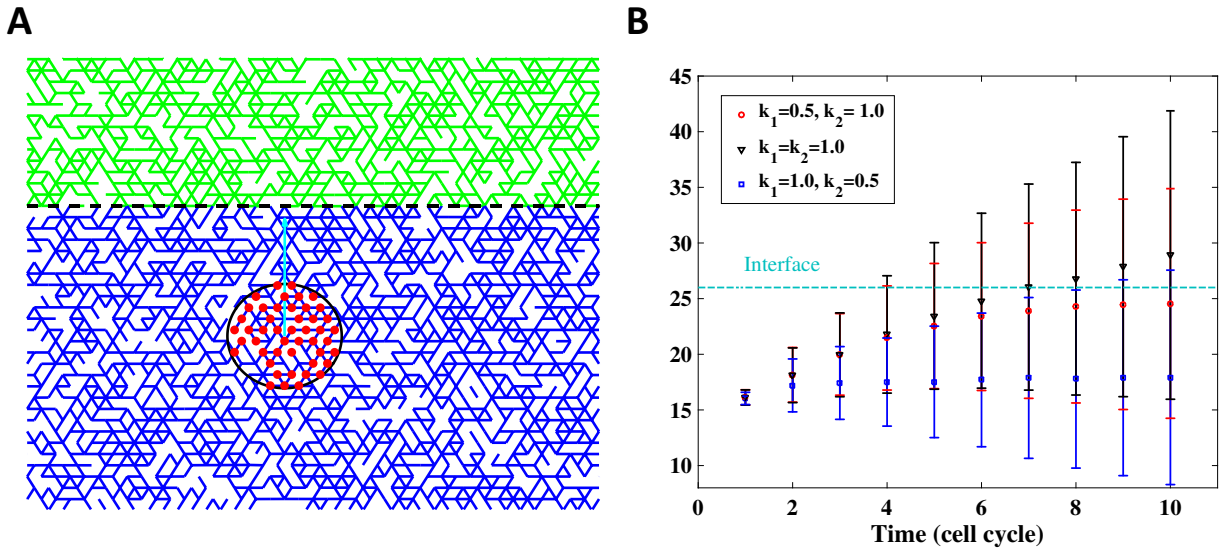

Fig. 10 Sharp interface created by varying spring constant k. (a) Initial configuration of the simulation. Green (Blue) bonds have a spring constant of $k_1(k_2)$. $p = 0.6$ and $\kappa/k = 0.001$. All other parameters are the same as in figure 8. (b) Average y coordinate of cells as a function of time. The red curve represents the results of moving from stiff region to soft region. The black curve represents the homogeneous case. And the blue curve represents from soft region to stiff region.

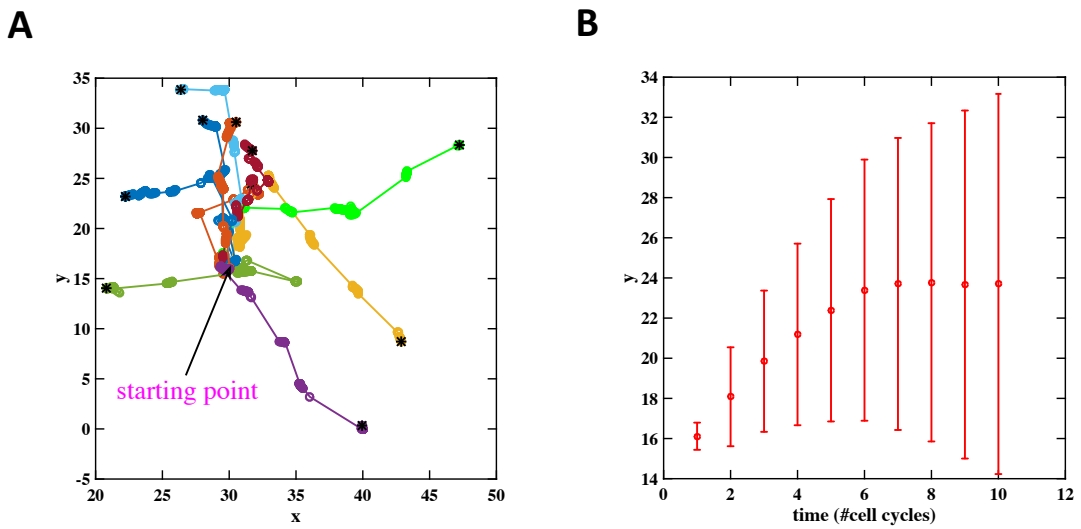

Fig. 11 Smooth change of stiffness created by varying spring constant k. The network size is 60 by 60. $k = 1$ for $y < 14$, $k = 0.2$ for $y > 38$. $k = 1 - 0.8 * (y - 14)/(38 - 14)$ for $y >= 14 \wedge y <= 38$ (a) Trajectory of cells under a uniform stiffness gradient. All cells start at (30, 16), with an initial orientation in the positive y-axis direction. Black stars indicates the ending position of cells after 10 cell cycles. (b) Average y coordinate of cells as a function of time

In summary, the aim of this paper was to show that a simple mechanical model is capable of explaining two important forms of mechanical steering, contact guidance and durotaxis. In reality, cell migration involves many complex biological processes that we have not considered. For instance, mechanical signaling can regulate cellular behaviors via signaling pathways[34,35]. Some cells can secret Matrix Metalloproteinases (MMPs) which can remodel extracellular matrix proteins[36]. In this work we simplify the problem by considering only mechanical aspects. Our model can serve as a framework for future work which incorporates biochemical signaling and other biological processes.

Conflicts of interest

There are no conflicts of interest to declare.

Acknowledgements

J.F and H.L. are supported by the National Science Foundation Center for Theoretical Biological Physics (Grant PHY-1427654). X.M. is supported by the National Science Foundation Grant NSF-DMR-1609051. H.L. is also supported in part by the Cancer Prevention and Research Institute of Texas Scholar Program of the State of Texas at Rice University.

Notes and references

1 C.-M. Lo, H.-B. Wang, M. Dembo and Y.-l. Wang, *Biophysical journal*, 2000, **79**, 144–152.

2 G. Charras and E. Sahai, *Nature reviews Molecular cell biology*, 2014, **15**, 813.

3 R. J. Pelham and Y.-l. Wang, *Proceedings of the National Academy of Sciences*, 1997, **94**, 13661–13665.

4 M. Raab, J. Swift, P. D. P. Dingal, P. Shah, J.-W. Shin and D. E. Discher, *J Cell Biol*, 2012, **199**, 669–683.

5 L. G. Vincent, Y. S. Choi, B. Alonso-Latorre, J. C. Del Álamo and A. J. Engler, *Biotechnology journal*, 2013, **8**, 472–484.

6 A. I. Teixeira, G. A. Abrams, P. J. Bertics, C. J. Murphy and P. F. Nealey, *Journal of cell science*, 2003, **116**, 1881–1892.

7 G. Dunn and T. Ebendal, *Experimental cell research*, 1978, **111**, 475–479.

8 A. D. Doyle, N. Carvajal, A. Jin, K. Matsumoto and K. M. Yamada, *Nature communications*, 2015, **6**, 8720.

9 C. A. R. Jones, L. Liang, D. Lin, Y. Jiao and B. Sun, *Soft Matter*, 2014, **10**, 8855–8863.

10 C. A. Jones, M. Cibula, J. Feng, E. A. Krnacik, D. H. McIntyre, H. Levine and B. Sun, *Proceedings of the National Academy of Sciences*, 2015, **112**, E5117–E5122.

11 D. Vader, A. Kabla, D. Weitz and L. Mahadevan, *PloS one*, 2009, **4**, e5902.

12 C. Storm, J. J. Pastore, F. C. MacKintosh, T. C. Lubensky and P. A. Janmey, *Nature*, 2005, **435**, 191.

13 J. Feng, H. Levine, X. Mao and L. M. Sander, *Physical Review E*, 2015, **91**, 042710.

14 J. Feng, H. Levine, X. Mao and L. M. Sander, *Soft matter*, 2016, **12**, 1419–1424.

15 M. Das, F. C. MacKintosh and A. J. Levine, *Phys. Rev. Lett.*, 2007, **99**, 038101.

16 C. P. Broedersz, X. Mao, T. C. Lubensky and F. C. MacKintosh, *Nat. Phys.*, 2011, **7**, 983–988.
17 X. Mao, O. Stenull and T. C. Lubensky, *Phys. Rev. E*, 2013, **87**, 042601.
18 M. Buenemann, H. Levine, W.-J. Rappel and L. M. Sander, *Biophysical journal*, 2010, **99**, 50–58.
19 R. Ananthakrishnan and A. Ehrlicher, *International journal of biological sciences*, 2007, **3**, 303–317.
20 C. P. McCann, E. C. Rericha, C. Wang, W. Losert and C. A. Parent, *PloS one*, 2014, **9**, e87981.
21 B. Harland, S. Walcott and S. X. Sun, *Physical biology*, 2011, **8**, 015011.
22 P. Krzyszczyk and C. W. Wolgemuth, *Biophysical journal*, 2011, **101**, L53–L55.
23 V. B. Shenoy, H. Wang and X. Wang, *Interface Focus*, 2015, **6**, 20150067–16.
24 M.-C. Kim, Y. R. Silberberg, R. Abeyaratne, R. D. Kamm and H. H. Asada, *Proceedings of the National Academy of Sciences of the United States of America*, 2018, **115**, E390–E399.
25 R. Meili, B. Alonso-Latorre, J. C. Del ï£ilamo, R. A. Firtel and J. C. Lasheras, *Molecular biology of the cell*, 2010, **21**, 405–417.
26 J. C. Del Alamo, R. Meili, B. Alonso-Latorre, J. Rodríguez-Rodríguez, A. Aliseda, R. A. Firtel and J. C. Lasheras, *Proceedings of the National Academy of Sciences*, 2007, **104**, 13343–13348.
27 G. I. Bell, *Science (New York, NY)*, 1978, **200**, 618–627.
28 B. J. DuChez, A. D. Doyle, E. K. Dimitriadis and K. M. Yamada, *Biophysj*, 2019, **116**, 670–683.
29 S. B. Lindström, D. A. Vader, A. Kulachenko and D. A. Weitz, *Physical Review E*, 2010, **82**, 051905.
30 K. M. Riching, B. L. Cox, M. R. Salick, C. Pehlke, A. S. Riching, S. M. Ponik, B. R. Bass, W. C. Crone, Y. Jiang, A. M. Weaver, K. W. Eliceiri and P. J. Keely, *Biophysj*, 2014, **107**, 2546–2558.
31 B. C. Isenberg, P. A. DiMilla, M. Walker, S. Kim and J. Y. Wong, *Biophysical journal*, 2009, **97**, 1313–1322.
32 M.-C. Kim, Y. R. Silberberg, R. Abeyaratne, R. D. Kamm and H. H. Asada, *Proceedings of the National Academy of Sciences*, 2018, 201717230.
33 J. Kim, J. Feng, C. A. Jones, X. Mao, L. M. Sander, H. Levine and B. Sun, *Nature communications*, 2017, **8**, 842.
34 D. E. Ingber, *Circulation research*, 2002, **91**, 877–887.
35 P. P. Provenzano and P. J. Keely, *J Cell Sci*, 2011, **124**, 1195–1205.
36 C. Legrand, C. Gilles, J.-M. Zahm, M. Polette, A.-C. Buisson, H. Kaplan, P. Birembaut and J.-M. Tournier, *The Journal of cell biology*, 1999, **146**, 517–529.